Geometric Phase-Driven Scattering Evolutions

Pengxiang Wang,[1] Yuntian Chen,[1,2,*] and Wei Liu[3,4,†]

[1]*School of Optical and Electronic Information, Huazhong University of Science and Technology, Wuhan, Hubei 430074, People's Republic of China*

[2]*Wuhan National Laboratory for Optoelectronics, Huazhong University of Science and Technology, Wuhan, Hubei 430074, People's Republic of China*

[3]*College for Advanced Interdisciplinary Studies, National University of Defense Technology, Changsha 410073, People's Republic of China*

[4]*Nanhu Laser Laboratory and Hunan Provincial Key Laboratory of Novel Nano-Optoelectronic Information Materials and Devices, National University of Defense Technology, Changsha 410073, People's Republic of China*

(Received 8 March 2024; accepted 16 July 2024; published 26 August 2024)

Conventional approaches for scattering manipulations largely rely on the technique of field expansions into spherical harmonics (electromagnetic multipoles), which nevertheless is not only nongeneric (expansion coefficients depend on the origin position of the coordinate system) but also more descriptive than predictive. Here, we explore this classical topic from a different perspective of controlled excitations and interferences of quasinormal modes (QNMs) supported by the scattering system. Scattered waves are expanded into coherent additions of QNMs, among which the relative amplitudes and phases are crucial factors to architect for scattering manipulations. Relying on the electromagnetic reciprocity, we provide full geometric representations based on the Poincaré sphere for those factors, and *discover the hidden geometric phase of QNMs* that drives the scattering evolutions. Further synchronous exploitations of the incident polarization-dependent geometric phase and excitation amplitudes enable efficient manipulations of both scattering intensities and polarizations. Continuous geometric phase spanning 2π is directly manifest through scattering variations, even in the rather elementary configuration of an individual particle scattering waves of varying polarizations. We have essentially established a profoundly all-encompassing framework for the calculations of geometric phase in arbitrary scattering systems that are reciprocal. Our theoretical model will greatly broaden horizons of many disciplines not only in photonics but also in general wave physics where geometric phase is generic and ubiquitous.

DOI: 10.1103/PhysRevLett.133.093801

The seminal topic of electromagnetic scatterings by particles has been the cornerstone for investigations of light-matter interactions and various scattering-related applications [1–7]. It has recently rapidly merged with other vibrant branches of singular, topological, and non-hermitian photonics [8–11]. Despite its rather long history and the aforementioned multidisciplinary advances, the central mathematical and physical technique for the field of particle scatterings remains to be spherical harmonics and electromagnetic multipolar expansions [1,12]. Indeed many breakthroughs in this field have been made based on this technique, such as recent introductions of Poincaré-Hopf theorem [13], electromagnetic multipolar parity [14], and duality [15] into Mie theory to reveal its intrinsic topological and geometric properties [16–20].

Nevertheless, the language of spherical harmonics and electromagnetic multipoles is more descriptive than predictive: except for some special scenarios of particles with ideal spherical or cylindrical symmetries, this technique describes the already known fields (either the near or scattered far fields calculated with other numerical methods) rather than predict them. For example, even for the elementary case of plane waves scattered by a particle of arbitrary shape, knowing the multipolar components of one scattering configuration barely tells anything about the scatterings of another even neighboring configuration with a slightly different incident direction and/or polarization. Moreover, the multipolar expansion coefficients are nongeneric and highly dependent on the origin position of the coordinate system chosen [1,12,15]. In addition, formalisms based on spherical harmonics are usually cumbersome and tend to obscure rather than clarify the profound physical picture. To circumvent all those limitations of the conventional method and further advance this seminal field, new concepts and techniques have to be introduced.

Here, we investigate the problem of electromagnetic scatterings from a different perspective of engineered quasinormal mode (QNM) [21,22] excitations and interferences. Scattered waves by the particles can be expanded into QNM radiations, and thus relative amplitudes and

*Contact author: yuntian@hust.edu.cn

†Contact author: wei.liu.pku@gmail.com

phases among them would decide the scattering patterns. Relying on the principle of reciprocity [23], we manage to provide full geometric representations for the excitation coefficients and discover the subtle geometric phase (Pancharatnam-Berry phase) [24–27] of QNMs. We further exploit the unveiled geometric phase and excitation amplitudes that are both dependent on incident polarizations for scattering manipulations, such as eliminating total and directional scatterings and designing directions of polarization singularities. Continuous geometric phases from $0-2\pi$ are directly manifest through scattering variations, even in the rather elementary configuration of an individual particle scattering plane waves of varying polarizations. Our work has essentially provided an exhaustive framework for the calculation of geometric phase in scattering systems, which can potentially accelerate both fundamental explorations and practical applications relying on scatterings, not only of electromagnetic waves, but also of waves of other forms where the geometric phase would generically emerge.

The eigenmodes supported by an arbitrary open scattering system, also termed as QNMs, can be directly calculated and they generally feature finite Q factors and complex eigenfrequencies [21,22,28]. When the system is excited by an external source, its scattered (near and far) fields can be expanded as

$$\mathbf{E}_{\mathrm{sca}}(\mathbf{r})=\sum_{m}\alpha_m\mathbf{E}_m(\mathbf{r}), \tag{1}$$

where $\mathbf{E}_m(\mathbf{r})$ denotes the radiation of the mth QNM and α_m is the complex expanding (excitation) coefficient. In the far field, both $\mathbf{E}_{\mathrm{sca}}(\mathbf{r})$ and $\mathbf{E}_m(\mathbf{r})$ are transverse, and thus Eq. (1) can be reformulated as $\mathrm{E}_{\mathrm{sca}}(\hat{\mathbf{r}})\mathbf{J}_{\mathrm{sca}}(\hat{\mathbf{r}})=\sum\alpha_m(\omega)\mathrm{E}_m(\hat{\mathbf{r}})\mathbf{J}_m(\hat{\mathbf{r}})$. Here, $\hat{\mathbf{r}}$ is unit direction vector $\hat{\mathbf{r}}=\mathbf{r}/|\mathbf{r}|$; $\mathrm{E}_{\mathrm{sca}}$ and E_m are field amplitudes; $\mathbf{J}_{\mathrm{sca}}(\hat{\mathbf{r}})$ and $\mathbf{J}_m(\hat{\mathbf{r}})$ are the corresponding unit Jones (row) vectors [29]. Both scattering intensity and polarization distributions are dictated by the relative amplitudes and phases among the excitation coefficients α_m, which are then decided by the incident wave (initial condition) [28]. Except for particles with high symmetries (such as spherical and cylindrical particles), conventional calculations of α_m rely on near-field integrations [21,22,30], the complexities of which have obscured the profound physical picture.

For an incident (along $\hat{\mathbf{r}}_{\mathrm{i}}$) plane wave of wavelength λ and polarization Jones vector $\mathbf{J}_{\mathrm{i}}$, if the scattering system is reciprocal, it was recently revealed that α_m can be alternatively calculated in the far field [30],

$$\alpha_m\propto\mathbf{J}_{\mathrm{i}}\mathbf{J}_m^{\dagger}(-\hat{\mathbf{r}}_{\mathrm{i}}), \tag{2}$$

where $\dagger$ denotes combined operations of complex conjugate and transpose, and thus $\mathbf{J}_m^{\dagger}(-\hat{\mathbf{r}}_{\mathrm{i}})$ is the corresponding column Jones vector for the QNM radiation opposite to the incident direction. To reveal the central principles, we start with the simplest scenario of two-QNM (denoted by modes A and B) excitations and the framework established can be naturally generalized to deal with multimode cases. To compact the notations, we simplify $\mathbf{J}_{\mathrm{A,B}}(-\hat{\mathbf{r}}_{\mathrm{i}})$ as $\mathbf{J}_{\mathrm{A,B}}$ and the Jones vector for QNM radiation along an arbitrary direction $\hat{\mathbf{r}}$ as $\mathbb{J}_{\mathrm{A,B}}$, with the direction vector $\hat{\mathbf{r}}$ suppressed for both Jones vectors and field vectors. Then according to Eqs. (1) and (2), the scattered field is [26,33,34]

$$\mathbf{E}_{\mathrm{sca}}\propto|\mathbf{J}_{\mathrm{i}}\mathbf{J}_{\mathrm{A}}^{\dagger}|\mathbf{E}_{\mathrm{A}}\exp(i\varphi_A)+|\mathbf{J}_{\mathrm{i}}\mathbf{J}_{\mathrm{B}}^{\dagger}|\mathbf{E}_{\mathrm{B}}\exp(i\varphi_B). \tag{3}$$

To geometrize the relative excitation amplitude and phase, we map the Jones vectors of $\mathbf{J}_{\mathrm{i}}$, $\mathbf{J}_{\mathrm{A}}$ ($\mathbb{J}_{\mathrm{A}}$), and $\mathbf{J}_{\mathrm{B}}$ ($\mathbb{J}_{\mathrm{B}}$) to points P, A($\mathbb{A}$), B($\mathbb{B}$) on the Poincaré sphere [26,29,33,34] of unit radius and parametrized by three Stokes parameters $S_{1,2,3}$ [shown in Fig. 1(a)]. Then Eq. (3) can be reduced to a pure geometric form [28]

$$\mathbf{E}_{\mathrm{sca}}\propto\cos\left(\frac{1}{2}\widehat{\mathrm{PA}}\right)\mathbf{E}_{\mathrm{A}}+\cos\left(\frac{1}{2}\widehat{\mathrm{PB}}\right)\mathbf{E}_{\mathrm{B}}\exp(i\varphi_g). \tag{4}$$

Here, $\widehat{\mathrm{PA}}$($\widehat{\mathrm{PB}}$) denotes the length of the great arc (shorter segment) connecting PA (PB); for example, when the incident polarization is orthogonal to that of mode A ($\mathbf{J}_{\mathrm{i}}\mathbf{J}_{\mathrm{A}}^{\dagger}=0$), P and A are antipodal points ($\widehat{\mathrm{PA}}=\pi$) and thus mode A would not be excited [$\cos(\frac{1}{2}\widehat{\mathrm{PA}})=0$], being consistent with the special scenario of single-mode excitations [30,31]. The phase contrast $\varphi_g=\varphi_B-\varphi_A$ can be expressed as a geometric phase [28]: $\varphi_g=\frac{1}{2}\Omega$, where Ω denotes the solid angle of the geodesic circuit PABP [see Fig. 1(a); Ω is positive (negative) for counterclockwise (clockwise) circuit viewed above [24–27].

Relying on Eq. (4), the scattering intensity $I_{\mathrm{sca}}=|\mathbf{E}_{\mathrm{sca}}|^2$ [28] and polarization along arbitrary directions can be calculated. When the scattered field $\mathbf{E}_{\mathrm{sca}}$ is projected to a specific polarization [point Q on the Poincaré sphere with Jones vector $\mathbf{J}_{\mathrm{Q}}$; see Fig. 1(a)], such as being analyzed by a polarizer, we obtain

$$\mathbf{E}_{\mathrm{sca}}^{Q}\propto\mathbf{J}_{\mathrm{Q}}\left[\cos\left(\frac{1}{2}\widehat{\mathrm{PA}}\right)\cos\left(\frac{1}{2}\widehat{\mathbb{A}\mathrm{Q}}\right)\mathrm{E}_{\mathrm{A}}+\cos\left(\frac{1}{2}\widehat{\mathrm{PB}}\right)\cos\left(\frac{1}{2}\widehat{\mathbb{B}\mathrm{Q}}\right)\mathrm{E}_{\mathrm{B}}\exp[i(\varphi_g+\varphi_g')]\right]. \tag{5}$$

Here, the extra geometric phase term comes from the polarization projection $\varphi_g'=\frac{1}{2}\Omega'$, where Ω' denotes the solid angle of the geodesic circuit $\mathbb{A}\mathrm{Q}\mathbb{B}\mathbb{A}$ [see Fig. 1(a)] [26,33,34]. The total geometric phase $\varphi_G=\varphi_g+\varphi_g'$ has to be calculatedly through two separate parts, unless A (B) and $\mathbb{A}$ ($\mathbb{B}$) overlap (QNM polarizations along $-\hat{\mathbf{r}}_{\mathrm{i}}$ and $\hat{\mathbf{r}}$ are identical), when it is half the solid angle of the whole geodesic circuit PAQBP.

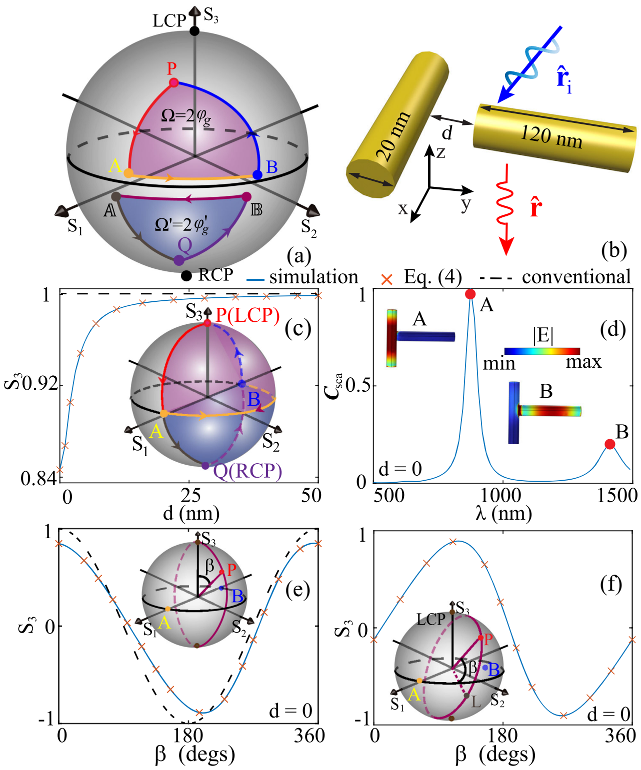

FIG. 1. (a) Poincaré sphere on which P (Q), A (𝔸) and B (𝔹) represent respectively the incident (projected) polarization and polarizations of the mode radiations opposite to the incident direction (along the scattering direction $\hat{\mathbf{r}}$). The geometric phase upon incident coupling (scattered polarization projection) is half solid angle of geodesic ciruit PABP (𝔸Q𝔹𝔸): $\varphi_g = \frac{1}{2}\Omega$ ($\varphi'_g = \frac{1}{2}\Omega'$). (b) A pair of perpendicular gold cylinders. Dependence of S_3 for scatterings along $-\mathbf{z}$ on inter-particle distance d (c), and incident polarizations transversing a great circle parameterized by β [(e) perpendicular incidence with $\hat{\mathbf{r}}_i$ along $-\mathbf{z}$; (f) tilted incidence with $\hat{\mathbf{r}}_i \perp \mathbf{x}$ and $\angle \hat{\mathbf{r}}_i \mathbf{y} = \pi/4$]. (d) Scattering spectra for LCP incidence along $-\mathbf{z}$, where the near fields of the two QNMs excited are shown as insets. In (d)–(f) $d = 0$ and in (c), (e) & (f) the incident wavelength $\lambda = 0.8$ μm and A (B) locates at $S_1 = 1$ ($S_1 = -1$) except that in (f) B locates at (−0.92, 0.316, −0.236).

We emphasize that the theoretical framework that has been so far elaborated on is fully based on the QNMs of open photonic systems, and thus is broadly applicable to scattering bodies (individual or clustered) of arbitrary geometric shapes and optical parameters, requiring only the reciprocity that guarantees the validity of Eq. (2). Furthermore, the geometric phase involved consists of two parts that have different origins: φ_g originates from the coupling of incident polarization (P) onto the QNM radiation polarizations (A and B) along $-\hat{\mathbf{r}}_i$ [Eq. (2)], while φ'_g originates from the projections of QNM radiation polarizations along an arbitrary scattering direction $\hat{\mathbf{r}}$ (𝔸 and 𝔹) to any desired polarization of interest (Q). Since the formalisms have put no constraints on $\hat{\mathbf{r}}_i$ or $\hat{\mathbf{r}}$, our model is applicable to arbitrary incident and scattering directions [28]. For applications that do not involve the scattering polarization projection, Eq. (4) contains all scattering information and φ'_g will be absent.

We now turn to a specific bicylinder scattering configuration shown in Fig. 1(b) to verify our theoretical framework (numerical calculations are performed using COMSOL Multiphysics throughout this work). The cylinders are identical, perpendicular to each other and consists of gold (effective permittivity fitted from data in Refs. [28,32]). The individual cylinder supports an electric dipole (ED) at the spectral regime of interest [28]. Similar structures consisting of optical items with spatially varying orientations are widely employed for various photonic functionalities based on geometric phase [35–38]. The mostly widely discussed scattering configuration is shining, for example, left-handed circularly polarized (LCP and $S_3 = 1$) waves along $-\mathbf{z}$ and then project the forward scattered waves onto right-handed circularly-polarized (RCP and $S_3 = -1$) states. The conventional pictorial representation of the geometric phase ($\varphi_G = \pi$) is shown in the inset of Fig. 1(c) [28]. From the perspective of our theoretical framework, such a representation is a reduced approximation of our model with the following two requirements: (i) each consisting cylinder supports an ED, with radiation polarizations along $\pm\mathbf{z}$ being both linear and parallel to the cylinder orientations; (ii) the couplings between the cylinders are negligible, ensuring that the EDs supported by both cylinders are also the QNMs of the bicylinder system. (i) and (ii) results in overlapped A (B) with 𝔸 (𝔹) on the equator of the Poincaré sphere, and thus the conventional representation [28] [inset of Fig. 1(c)] is merely a special scenario of the our general representation in Fig. 1(a). However, when the modes supported are not EDs, the coupling is not negligible, or the incident and scattering directions are arbitrary, the conventional methodology to calculate geometric phase relying on structural orientations would break down.

To showcase the superiority of our model, we show in Fig. 1(c) the evolution of the polarization (in terms of S_3) for the forward scatterings along $-\mathbf{z}$ with fixed LCP incidence while varying intercylinder distance d. For the conventional approach, the RCP components cancel each other due to destructive interference ($\varphi_G = \pi$) and thus the forward scattered waves maintain to be LCP with fixed $S_3 = 1$ [28]. Nevertheless, as is manifest in Fig. 1(c), with decreasing d and thus stronger intercylinder couplings, the forward scattered waves will contain both RCP and LCP components, which our model accurately reproduces. For the extreme case of $d = 0$, we further show in Fig. 1(d) the scattering cross section (C_{sca}) spectra to confirm the excitations of two QNMs (LCP incidence), near fields of which are shown as insets. The QNM radiations along the opposite incident direction ($+\mathbf{z}$) are linear [28] and their positions are indicated in the inset of Fig. 1(e), where we show the forward scattering polarization evolutions with varying incident polarizations. Here, P locates on a great circle parametrized by β ($\beta = 0$ for LCP incidence) and equally bisects $\widehat{\mathrm{AB}}$ ($\widehat{\mathrm{PA}} = \widehat{\mathrm{PB}}$). We then tilt the incident direction ($\hat{\mathbf{r}}_{\mathrm{i}} \perp \mathbf{x}$ and $\angle \hat{\mathbf{r}}_{\mathrm{i}}\mathbf{y} = \pi/4$) and show the scattering polarization along $-\mathbf{z}$ in Fig. 1(f) for P transversing another great circle equally bisecting $\widehat{\mathrm{AB}}$ (see the inset; $\beta = 0$ corresponds to state L that locates on $\widehat{\mathrm{AB}}$ with $\varphi_g = 0$). Since radiation of mode B opposite to the incident direction is not linearly polarized anymore, B does not locate on the equator. For both scenarios of perpendicular and tilt incidences [Figs. 1(e) and 1(f)], results from our model agree perfectly well with the simulation results. The results for the nonperpendicular bicylinder configuration and for another classical structure consisting of a pair of twisted split-ring resonators [28] further confirm the validity of our theoretical model.

In our theoretical framework, the calculation of the geometric phase has nothing to do with orientations of the structures, and thus our model is applicable to individual particles without any preferred orientations. The gold particle shown in Fig. 2(a) exhibits fourfold rotation symmetry that secures a pair of degenerate QNMs [28]. We shine plane waves along $+\mathbf{z}$ and track scattering intensity distributions on the $\mathbf{x}$-$\mathbf{y}$ plane. The radiations of the two QNMs along $-\mathbf{z}$ (opposite to the incident direction) are almost linearly polarized parallel to $\mathbf{x}$ and $\mathbf{y}$ [see points A and B in Fig. 2(b)] [28]. The normalized scattering intensity distributions [parametrized by the azimuthal angle ϕ as shown in Fig. 2(a)] are shown in Figs. 2(c) and 2(d), for four incident polarizations with the corresponding geometric phase [Fig. 2(b)] $\varphi_g \approx 0, \pi$ (two perpendicular linear polarizations) and $\varphi_g \approx \pi/2, \pi/4$ (circular and elliptical polarizations), respectively. In Fig. 2(c), the geometric phase π is directly manifest through the two distinct scattering patterns and we note that our demonstration (with an individual scattering particle) of such classical geometric phase is even simpler and more direct than the earliest ones by Fresnel-Arago and Hamilton-Lloyd [27]. As is shown in Fig. 2(c), for $\varphi_g \approx 0$ the scattering along the direction $\phi = \phi_0 \approx 113°$ is zero. Along this direction, according to Eq. (4) we have $\mathbf{E}_{\mathrm{A}} \approx -\mathbf{E}_{\mathrm{B}}$ since $\widehat{\mathrm{PA}} \approx \widehat{\mathrm{PB}} \approx \pi/2$ and $\varphi_g \approx 0$ [Fig. 2(b)]. With fixed $\widehat{\mathrm{PA}} \approx \widehat{\mathrm{PB}}$ while changing φ_g, we then have $\mathbf{E}_{\mathrm{sca}} \propto 1 - \exp(i\varphi_g)$ and thus scattering intensity along this direction: $I_{\mathrm{sca}} \propto |\mathbf{E}_{\mathrm{sca}}|^2 \propto 1 - \cos(\varphi_g)$. We then show the evolutions of $I_{\mathrm{sca}}(\phi = \phi_0)$ on such a polarization great circle ($S_1 = 0$) parametrized by $\beta \in [0, 2\pi]$, as shown in the inset in Fig. 2(e). Obviously the solid angle $\Omega = 2\beta$ and $\varphi_g = \beta$ [Fig. 2(b)], and thus the evolution observe the relation $I_{\mathrm{sca}}(\phi = \phi_0) \propto 1 - \cos(\beta)$, which agrees perfectly with the numerical results included in Fig. 2(e).

The polarization distributions on the $\mathbf{x}$-$\mathbf{y}$ plane are further shown in Fig. 3(a), for linear polarization ($S_2 = 1$ and $\varphi_g \approx 0$) and LCP ($S_3 = 1$ and $\varphi_g \approx \pi/2$)

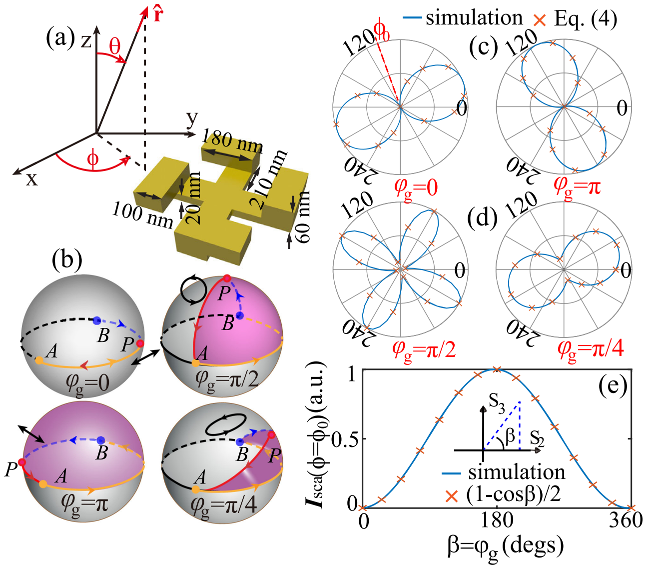

FIG. 2. (a) A gold particle with fourfold rotation symmetry and a spherical coordinate system parameterized by $\mathbf{r} = (r, \theta, \phi)$. Scattering intensity distributions on the $\mathbf{x}$-$\mathbf{y}$ plane with P locating at (0, 1, 0) and (0, -1, 0) for (c), which correspond to two orthogonal incident linear polarizations [polarized along $\phi = \pi/4$ ($S_2 = 1$) and polarized along $\phi = 3\pi/4$ ($S_2 = -1$)]; locating at (0, 0, 1) and (0, $\sqrt{2}/2$, $\sqrt{2}/2$) for (d), which correspond to LCP incident and elliptic incident polarization. The geometric phases are, respectively, $\varphi_g = 0, \pi, \pi/2$ and $\pi/4$, as shown in (b). In (c) one direction of zero scattering $\phi = \phi_0 \approx 113°$ is specified. (e) The dependence of $I_{\mathrm{sca}}(\phi = \phi_0)$ on β (see the inset). In (c)–(e) the incident wavelength $\lambda = 2.34$ μm.

incidences. According to Eq. (4), the locations of circularly polarized scatterings ($S_3 = \pm 1$; circular polarization singularities [39]) can be directly predicted and even designed by selecting proper incident polarization and directions. We show the scattering polarization distributions (simulated results) on the whole scattering momentum sphere in Fig. 3(b) for the linear polarization incidence ($S_2 = 1$) and the predicted locations of polarization singularities are also marked by crosses, agreeing well with the numerical calculations.

Also according to Eq. (4), there is a rather interesting scenario of overlapped A and B: directions along which the radiation polarizations for both QNMs are the same. For waves incident opposite to those directions, we have $\cos(\frac{1}{2}\widehat{\mathrm{PA}}) = \cos(\frac{1}{2}\widehat{\mathrm{PB}})$ and $\varphi_g = 0$ [see Fig. 1(a)]. This results in fixed scattering polarization along any direction, irrespective of varying incident polarizations. For the marked direction ($\phi = \phi_0$) in Fig. 2(c), as has been discussed, QNM radiation polarizations are the same. We denote this direction as $\hat{\mathbf{r}}_{\mathrm{A=B}}$ and shine opposite to it ($\hat{\mathbf{r}}_{\mathrm{i}} = -\hat{\mathbf{r}}_{\mathrm{A=B}}$) LCP and RCP waves. We then track the scattering polarization variation on the whole momentum sphere through the parameter $|\mathbf{J}_{\mathrm{sca}}^{\mathrm{LCP}}(\mathbf{J}_{\mathrm{sca}}^{\mathrm{RCP}})^{\dagger}|$, where $|\mathbf{J}_{\mathrm{sca}}^{\mathrm{LCP}}(\mathbf{J}_{\mathrm{sca}}^{\mathrm{RCP}})^{\dagger}| = 1$ means the scattering polarization does

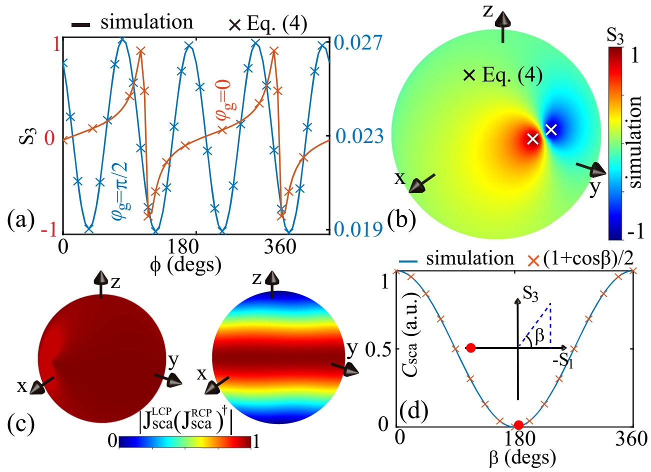

FIG. 3. (a) S_3 distributions on the **x**-**y** plane with P locating at (0, 0, 1) and (0, 1, 0), with $\varphi_g = \pi/2$ and 0, respectively. (b) S_3 distributions on the whole scattering momentum sphere for P locating at (0, 1, 0), on which the predicted directions of circular polarization singularities are marked by crosses. (c) Distributions of $|\mathbf{J}^{\mathrm{LCP}}_{\mathrm{sca}}(\mathbf{J}^{\mathrm{RCP}}_{\mathrm{sca}})^\dagger|$ for waves incident along $\hat{\mathbf{r}}_{\mathrm{i}} = -\hat{\mathbf{r}}_{\mathrm{A=B}}$ (left) and $\hat{\mathbf{r}}_{\mathrm{i}} = +\mathbf{z}$ (right). (d) Variations of C_{sca} for P transversing a great circle ($S_2 = 0$), covering matched polarization ($\beta = 0$), orthogonal polarization (marked; $\beta = \pi$), and LCP and RCP ($\beta = \pi/2$ and $3\pi/2$). The incident wavelength $\lambda = 2.34$ μm.

not change for RCP and LCP incidences [see Fig. 3(c)]. For comparison, we also shine circularly polarized waves along $+\mathbf{z}$ (opposite to which the QNM radiations are distinct and thus A and B do not overlap) and show its $|\mathbf{J}^{\mathrm{LCP}}_{\mathrm{sca}}(\mathbf{J}^{\mathrm{RCP}}_{\mathrm{sca}})^\dagger|$ distribution in Fig. 3(c), confirming that for general incident directions the scattering polarizations are dependent on incident polarizations.

Another interesting property for overlapped A and B is that the incident polarization can be tuned to be orthogonal to that of both QNMs [$\cos(\frac{1}{2}\widehat{\mathrm{PA}}) = \cos(\frac{1}{2}\widehat{\mathrm{PB}}) = 0$; $\mathbf{E}_{\mathrm{sca}} = 0$ in Eq. (4)]. For such an incident polarization, neither QNM would be excited and thus the particle would become invisible. For the same incident direction ($\hat{\mathbf{r}}_{\mathrm{i}} = -\hat{\mathbf{r}}_{\mathrm{A=B}}$), we show the evolutions of scattering cross sections with varying incident polarizations in Fig. 3(d). The incident polarization traverses a great circle, covering matched polarization ($\beta = \widehat{\mathrm{PA}} = \widehat{\mathrm{PB}} = 0$), LCP ($\beta = \pi/2$), orthogonal polarization ($\beta = \widehat{\mathrm{PA}} = \widehat{\mathrm{PB}} = \pi$). According to Eq. (4) with $\varphi_g = 0$ and $\widehat{\mathrm{PA}} = \widehat{\mathrm{PB}} = \beta$: $\mathbf{E}_{\mathrm{sca}} \propto (\mathbf{E}_{\mathrm{A}} + \mathbf{E}_{\mathrm{B}})\cos(\beta/2)$; that is, scattering along any direction and thus also the scattering cross section would satisfy $I_{\mathrm{sca}}, C_{\mathrm{sca}} \propto \cos^2(\beta/2) = [1 + \cos(\beta)]/2$, which is verified by Fig. 3(d). We note that the scattering evolutions in Fig. 2(e) are driven by changing φ_g with fixed $\widehat{\mathrm{PA}} = \widehat{\mathrm{PB}}$ [as is also the case for those in Figs. 1(e) and 1(f)], while those in Fig. 3(d) driven by changing $\widehat{\mathrm{PA}} = \widehat{\mathrm{PB}} = \beta$, with fixed $\varphi_g = 0$.

In conclusion, we have unveiled the hidden and subtle geometric phase of QNMs and reveal how they drive scattering evolutions with varying incident polarizations. The geometric phase can be exploited to efficiently manipulate the scatterings, such as scattering eliminations and polarization singularity generations. For the general scenario of more than two QNMs being simultaneously excited, the relative amplitude and phase among any two QNMs can be calculated and then calculations for interferences among all QNMs become standard procedures. This means that the theoretical framework we have constructed is generic and broadly applicable. We have essentially established a profoundly comprehensive framework to calculate geometric phases in scattering systems, and unlocked an extra hidden dimension for electromagnetic scattering manipulations. Similar dimensions might be uncovered for waves of other forms for which geometric phase is generic and ubiquitous, providing new flexibilities for many physics and interdisciplinary branches that are related to wave scatterings.

Acknowledgments—This work is supported by National Natural Science Foundation of China (Grants No. 11874426 and No. 61405067), Outstanding Young Researcher Scheme of Hunan Province (2024JJ2056), and several Researcher Schemes of National University of Defense Technology. W. L. acknowledges many illuminating correspondences with Sir Michael Berry.

[1] C. F. Bohren and D. R. Huffman, *Absorption and Scattering of Light by Small Particles* (Wiley, New York, 1983).
[2] A. I. Kuznetsov, A. E. Miroshnichenko, M. L. Brongersma, Y. S. Kivshar, and B. Luk'yanchuk, Optically resonant dielectric nanostructures, Science **354**, aag2472 (2016).
[3] W. Liu and Y. S. Kivshar, Generalized Kerker effects in nanophotonics and meta-optics [Invited], Opt. Express **26**, 13085 (2018).
[4] A. Krasnok, D. Baranov, H. Li, M.-A. Miri, F. Monticone, and A. Alú, Anomalies in light scattering, Adv. Opt. Photonics **11**, 892 (2019).
[5] Y. Kivshar, The rise of Mie-tronics, Nano Lett. **22**, 3513 (2022).
[6] H. Altug, S.-H. Oh, S. A. Maier, and J. Homola, Advances and applications of nanophotonic biosensors, Nat. Nanotechnol. **17**, 5 (2022).
[7] S. Fan and W. Li, Photonics and thermodynamics concepts in radiative cooling, Nat. Photonics **16**, 182 (2022).
[8] W. Liu, W. Liu, L. Shi, and Y. Kivshar, Topological polarization singularities in metaphotonics, Nanophotonics **10**, 1469 (2021).
[9] M.-A. Miri and A. Alù, Exceptional points in optics and photonics, Science **363**, eaar7709 (2019).
[10] K. Koshelev, A. Bogdanov, and Y. Kivshar, Meta-optics and bound states in the continuum, Sci. Bull. **64**, 836 (2019).
[11] M. Kang, T. Liu, C. T. Chan, and M. Xiao, Applications of bound states in the continuum in photonics, Nat. Rev. Phys. **5**, 659 (2023).

[12] A. Doicu, T. Wriedt, and Y. A. Eremin, *Light Scattering by Systems of Particles: Null-Field Method with Discrete Sources: Theory and Programs* (Springer, New York, 2006), Vol. 124.

[13] T. Needham, *Visual Differential Geometry and Forms: A Mathematical Drama in Five Acts* (Princeton University Press, Princeton, NJ, 2021).

[14] W. Liu, J. Zhang, B. Lei, H. Ma, W. Xie, and H. Hu, Ultra-directional forward scattering by individual core-shell nanoparticles, Opt. Express **22**, 16178 (2014).

[15] J. D. Jackson, *Classical Electrodynamics Third Edition*, 3rd ed. (Wiley, New York, 1998).

[16] W. Liu, Generalized magnetic mirrors, Phys. Rev. Lett. **119**, 123902 (2017).

[17] W. Chen, Y. Chen, and W. Liu, Singularities and Poincaré indices of electromagnetic multipoles, Phys. Rev. Lett. **122**, 153907 (2019).

[18] W. Chen, Y. Chen, and W. Liu, Line singularities and Hopf indices of electromagnetic multipoles, Laser Photonics Rev. **14**, 2000049 (2020).

[19] I. Fernandez-Corbaton, X. Zambrana-Puyalto, N. Tischler, X. Vidal, M. L. Juan, and G. Molina-Terriza, Electromagnetic duality symmetry and helicity conservation for the macroscopic Maxwell's equations, Phys. Rev. Lett. **111**, 060401 (2013).

[20] Q. Yang, W. Chen, Y. Chen, and W. Liu, Electromagnetic duality protected scattering properties of nonmagnetic particles, ACS Photonics **7**, 1830 (2020).

[21] P. Lalanne, W. Yan, K. Vynck, C. Sauvan, and J.-P. Hugonin, Light interaction with photonic and plasmonic resonances, Laser Photonics Rev. **12**, 1700113 (2018).

[22] A. Gras, P. Lalanne, and M. Duruflé, Nonuniqueness of the quasinormal mode expansion of electromagnetic Lorentz dispersive materials, J. Opt. Soc. Am. A **37**, 1219 (2020).

[23] C. Caloz, A. Alù, S. Tretyakov, D. Sounas, K. Achouri, and Z.-L. Deck-Léger, Electromagnetic nonreciprocity, Phys. Rev. Appl. **10**, 047001 (2018).

[24] S. Pancharatnam, Generalized theory of interference, and its applications, Proc. Indian Acad. Sci. **44**, 247 (1956).

[25] M. V. Berry, Quantal phase factors accompanying adiabatic changes, Proc. R. Soc. A **392**, 45 (1984).

[26] M. V. Berry, The adiabatic phase and Pancharatnam phase for polarized-light, J. Mod. Opt. **34**, 1401 (1987).

[27] M. Berry, A geometric-phase timeline, Opt. Photonics News **35**, 42 (2024).

[28] See Supplemental Material at http://link.aps.org/supplemental/10.1103/PhysRevLett.133.093801, which includes Refs. [1,27,29–32], for (i) relative amplitudes and phases among QNMs; (ii) complex eigenfrequencies and near fields of QNMs, and their scattered field intensity and polarization distributions on the momentum sphere; (iii) normalized Jones vectors and Stokes parameters for polarizations of QNM radiations opposite to the incident direction; (iv) selective QNM excitations; (v) nonperpendicular bicylinder scattering; (vi) twisted bi-SRR scattering; (vii) gain particle scattering; and (viii) conventional methodology to calculate geometric phase based on structural orientations.

[29] A. Yariv and P. Yeh, *Photonics: Optical Electronics in Modern Communications*, 6th ed. (Oxford University Press, New York, 2006).

[30] W. Chen, Q. Yang, Y. Chen, and W. Liu, Extremize optical chiralities through polarization singularities, Phys. Rev. Lett. **126**, 253901 (2021).

[31] C. Wen, J. Zhang, S. Qin, Z. Zhu, and W. Liu, Momentum-space scattering extremizations, Laser Photonics Rev. **18**, 2300454 (2024).

[32] P. B. Johnson and R. W. Christy, Optical constants of the noble metals, Phys. Rev. B **6**, 4370 (1972).

[33] G. N. Ramachandran and S. Ramaseshan, Crystal optics, in *Kristalloptik·Beugung/Crystal Optics·Diffraction*, Handbuch Der Physik/Encyclopedia of Physics, edited by S. Flügge (Springer, Berlin, Heidelberg, 1961), pp. 1–217.

[34] S. Pancharatnam, *Collected Works of S. Pancharatnam* (Oxford University Press for the Raman Research Institute, London, 1975).

[35] G. Li, S. Zhang, and T. Zentgraf, Nonlinear photonic metasurfaces, Nat. Rev. Mater. **2**, 17010 (2017).

[36] E. Cohen, H. Larocque, F. Bouchard, F. Nejadsattari, Y. Gefen, and E. Karimi, Geometric phase from Aharonov–Bohm to Pancharatnam–Berry and beyond, Nat. Rev. Phys. **1**, 437 (2019).

[37] C. P. Jisha, S. Nolte, and A. Alberucci, Geometric phase in optics: From wavefront manipulation to waveguiding, Laser Photonics Rev. **15**, 2100003 (2021).

[38] Y. Guo, M. Pu, F. Zhang, M. Xu, X. Li, X. Ma, and X. Luo, Classical and generalized geometric phase in electromagnetic metasurfaces, Photonics Insights **1**, R03 (2022).

[39] G. J. Gbur, *Singular Optics* (CRC Press Inc, Boca Raton, 2016).